# Front-end Circuits for Ultra-High-Frequency Underwater Acoustic Communication Systems

Fengyi Sun<sup>®</sup>, Xiyuan Zhu<sup>®</sup>, Yukang Xue<sup>®</sup>, Jinfeng Li<sup>®</sup>, and Y. Rosa Zheng<sup>®</sup>, The authors are with the Department of Electrical & Computer Engineering, Lehigh University, Bethlehem, PA 18015, USA, Email: {fes223, xiz418, yux615, jili18, yrz218}@lehigh.edu.

Abstract—This paper investigates the front-end circuits for ultra-high frequency underwater acoustic (UWA) transmitter and receiver. The transmitting front-end consists of an audio driver, a Class D power amplifier, and an impedance matching circuit. The receiver front-end consists of a multi-stage Low Noise Amplifier (LNA) with band-pass filtering and level shifting. The front-end circuits are made for 115 kHz, 160 kHz, 200 kHz and 400 kHz, respectively. Extensive lab and field tests demonstrate that the transmitter is capable of amplifying a Pulse Width Modulated (PWM) signal to 144 V to 280 V peak-to-peak and the receiver can achieve an amplification gain of 50 dB with 60 dB out band attenuation. The example 160 kHz system achieves a receiving Signal-to-Noise Ratio (SNR) of 3.5 dB over a distance of 1000 meters.

## I. INTRODUCTION

The majority of underwater acoustic communication operate in the frequency band below 40 kHz [1], [2]. because high frequency acoustic signals suffer strong frequency-dependent attenuation underwater. As the carrier frequency increases, the achievable communication distance decreases [3]. Typically, the frequency band below a few kilo-hertz is used for ultralong distance underwater communication of more than 100 km. The medium frequency band between 5 kHz to 20 kHz may achieve a communication distance of 10 km - 100 km; while the high-frequency band between 20 kHz - 50 kHz can reach a distance of a few kilometers. All of these systems require very high transmission power and may cause significant disturbance to marine animals using the same frequency bands for their echolocation. In recent years, more applications call for the Internet of Underwater Things (IoUT) technology [4] which may utilize ultra-high frequency band greater than 100 kHz with short communication distances. This type of acoustic communication systems can utilize wide bandwidth greater than 20 kHz and achieve high data rate on the order of 100 kbps [5]. In addition, these ultra-high-frequency systems require pretty low transmission power. Their circuits and transducers have small form factors. The material cost of such system can be significantly lower than conventional acoustic communication system too. Therefore, ultra-high-frequency acoustic communication systems are of particular interest to commercial applications such as underwater wireless cameras or video transmission [6].

This paper investigates the analog front-end circuits for underwater acoustic communication systems at 100 kHz – 400 kHz frequency bands. Commercial off-the-shelf products for

such frequency band are rarely available as typical acoustic communication systems use lower bands, and typical sonar systems and ultra-sound imaging systems use higher frequency bands greater than 500 kHz. The few related products in this frequency band include: the acoustic telemetry system [7] by Pacific Northwest National Laboratory (PNNL) and Advanced Tracking Systems (ATS) operating at 200 kHz or 400 kHz bands; the Evologic HS acoustic communication system operating at 120 kHz - 180 kHz band (https://evologics.de/ acoustic-modem/hs), and the HERMES modem in 260 kHz -380 kHz band [8]. Nevertheless, the front-end circuits of these systems are unavailable commercially. This work studies the existing front-end circuits and makes prototypes for transmitter and receiver front-end circuits. We modify the typical class D power amplifier designed for 30 kHz carrier frequency [9] and makes a PA to operate at 100 kHz - 400 kHz band for the transmitter frond-end circuit. We also modify the HEU's Low-Noise Amplifier (LNA) design and make separate receiver front-end prototypes for 100 kHz, 160 kHz, 200 kHz, and 400 kHz with 10% bandwidth bandpass filters.

Figure 1 shows the block diagram of the typical front-end circuits for underwater communication systems. The transmitter consists of the following parts: a controller generates the data bits to be transmitted; a digital modulator maps the bits to single-carrier or OFDM (Orthogonal Frequency-Division Multiplexing) symbols; a transmitting front-end circuit amplifies the passband modulated signal; and a projector converts the signal to an acoustic wave. Within the proposed transmitting front-end circuit, the isolator separates the digital signal from the analog signal. The audio amplifier amplifies the modulated PWM (Pulse Width Modulation) signal and generates its inversion with deadband protection. The class D power amplified further amplifies the PWM signal and the matching circuit provides the resonance with the transducer to achieve the desired transmission power and frequency response. The receiver contains the following parts: a low-noise amplifier (LNA) amplifies and band-pass filters the signal from the hydrophone; an analog to digital converter (ADC) converts the analog inputs to a digital signal; and a digital signal processor demodulates the signal to recover the information bits. The proposed LNA circuit consists of an instrumentation amplifier, a fixed-gain amplifier, a bandpass filter, and a level shifter.

This work conducts extensive lab and field tests on the transmitter and receiver front-end circuits. The results demonstrate

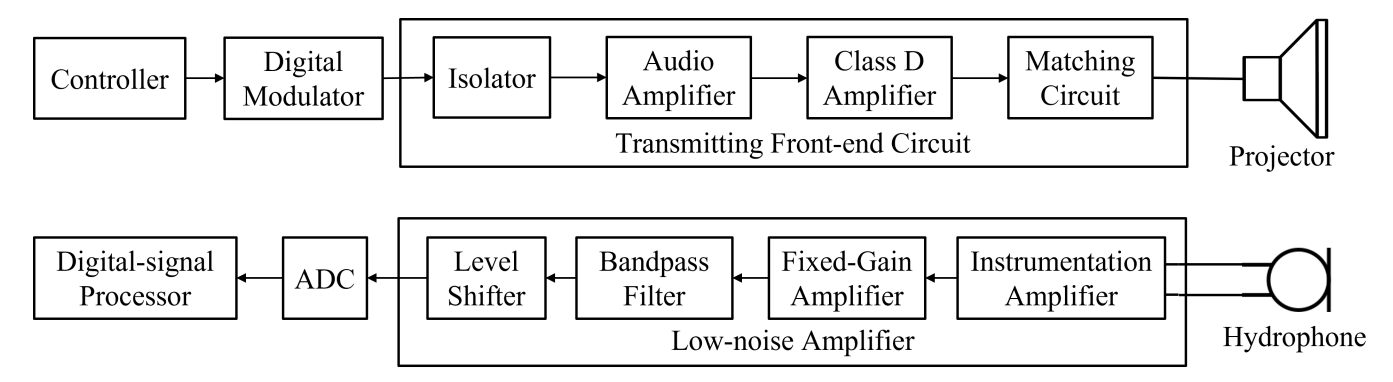


Fig. 1: Block diagram of an acoustic communication system with front-end circuits

that the transmitter is capable of amplifying a Pulse Width Modulated (PWM) signal to 144  $V_{pp}$  to 280  $V_{pp}$  as required by the 400 kHz – 100 kHz transducers. The receiver can achieve an amplification gain of 50 dB with 60 dB out band attenuation at 10% bandwidth. The example 160 kHz system achieves a receiving Signal-to-Noise Ratio (SNR) of 3.5 dB over a distance of 1000 meters.

#### II. TRANSMITTER FRONT END

The transmitter front-end circuit amplifies the PWM signals generated by the digital processor to drive the transducer for acoustic wave transmission. For very high frequency band greater than 200 kHz and short range communications, the transducers may require lower voltage and lower power. The PA circuit may use high-voltage analog switches [7], [10] for constant-modulo single-carrier modulation. However, class D PAs are commonly used to achieve higher power and better efficiency. This work uses the half-bridge class D amplifier as shown in Fig. 2.

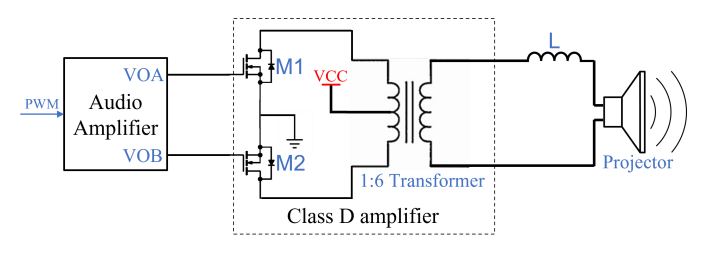


Fig. 2: A typical half-bridge Class D amplifier with its input driver and output load matching circuit

A typical half-bridge class D power amplifier consists of two MOSFETs [11] which are called high-side and low-side switches, respectively. They serve as push-pull converter by alternatively turning on and off and they have to be turned on at different times. When the high-side MOSFET is turned on, the current flows from VCC through the high-side primary coil of the transformer. Similarly, when the low-side MOSFET is turned on, the current flows through the low-side primary coil. The voltage on MOSFETs' drain-pins switches between high voltage (+ $V_{cc}$ ) and ground (GND). The peak-to-peak voltage

between the two drain pins of the MOSFETs is twice of  $V_{cc}$ , as shown in Fig. 3.

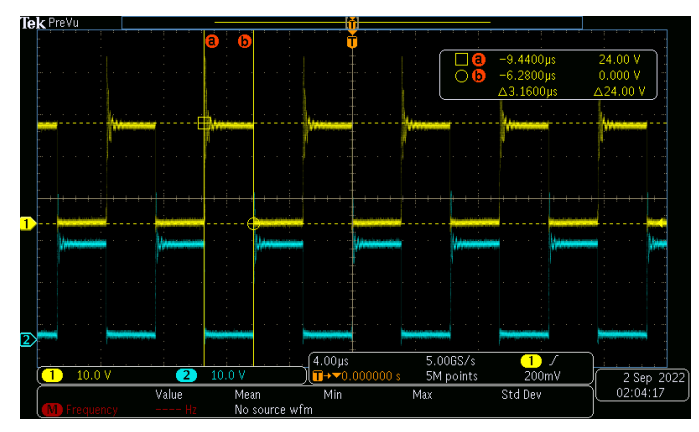


Fig. 3: Voltage on the MOSFET drains

This voltage from the drain-pins of the MOSFETs supplies to the transformer as the primary voltage. Since the two primary coils are wound in the same direction and with the same number of turns  $N_1$ , the secondary coil with  $N_2$  turns has an output voltage

$$V_{out} = \frac{N_2}{N_1} (V_1 - V_2)$$

where  $V_1$  and  $V_2$  are the voltages at the drain terminals of the two MOSFETs, respectively.

The half-bridge class D amplifier is driven by an audio amplifier at the input. The audio amplifier accepts the input PWM signal and convert it into the high-side and low-side switching signals VOA and VOB. Commercial audio amplifier Si8241BB can amplify a 0-3 V PWM and generate the high-side and low-side switch drivers VOA and VOB at 12 V. The audio amplifier also inserts the dead time at the turn-on edges of both the high-side and the low-side signals. The built-in dead time prevents the two MOSFETs from being turned on at the same time, which increases power efficiency and prevents device damage. A large dead time would cause high Total Harmonic Distortion (THD) and a too-short dead time would result in Shoot Through Current which may damage

the devices [11]. A resistor connecting to Si8241BB pin 6 can adjust the dead time from 400 ps to 1000 ns. In the proposed design, a 3.9 k $\Omega$  resistor is picked for 39 ns of dead time. The lab testing of dead time is present in Fig. 4, where the dead time is measured as 36.2 ns .

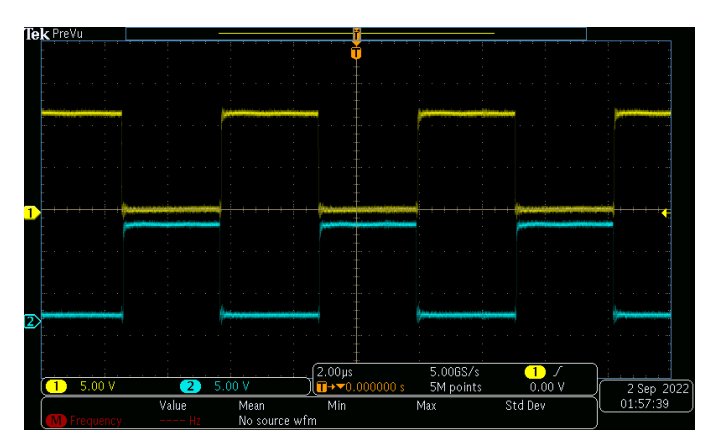


Fig. 4: Outputs of the audio driver VOA (yellow line) and VOB (blue line)

To adopt a class D amplifier for the very high-frequency band, MOSFETs with very high switching frequencies have to be used. For commercial audio band class D amplifiers, the NMOS-FET IRF540 is commonly used [11]. The MOSFET turns on in the linear region and turns off in the cut-off region. However, switching between on and off state contains time delays. A total of four time delays measure the switching time of the MOSFETs. 1) The input capacitance  $C_{iss}$  needs to charge to the threshold voltage to turn on, which is the turn-on delay. 2) Rise time refers to the gate charging time from threshold voltage to gate voltage when the drain current is fully conductive. 3) The time required to discharge the gate capacitance to the active gate control region is the turnoff delay. 4) The fall time is the time delay for the input capacitance to discharge to the gate threshold voltage[12, P. 123]. To turn on or off a MOSFET faster, the total gate charges  $Q_q$  required to turn on/off the MOSFET has to be smaller[13]. However a smaller  $Q_g$  usually means a larger ON resistance  $R_{DS}$  which reduces the power efficiency of the class D amplifier. The IRF540 has  $Q_q = 72$  nC and  $R_{DS} = 77m\Omega$ at  $V_{GS} = 10$  V, which works fine for frequency band less than 100 kHz. For ultra-high-frequency band greater than 100 kHz, we choose the MOSFET FDD86326 [14] which has a much smaller  $Q_g$  and ON resistor:  $Q_g=13.4~{\rm nC}$  — 19 nC and ,  $R_{DS}=23m\Omega$  at  $V_{GS}=10$ , which are much smaller than those of IRF540. The switching times of FDD86326 are also much shorter than that of IRF540.

The transformer in our prototype is hand-made with 24 AWG magnetic wire and TDK P18  $\times$  11 ferrite cores and accessories. We select  $N_1=10$  and  $N_2=60$ . If  $V_{cc}=12$  V to 24 V, then the transformer would boost the output voltage to 144 V to 288 V which are sufficient for the 100 kHz – 400 kHz transducers.

TABLE I: Transducer capacitance (C), matching inductance (L), and number of turns (N) for different frequencies

Frequency	$A_L$ (nH/turns <sup>2</sup> )	C (nF)	L (μH)	N	L-measured
115 kHz	4000	4.305	444.90	11	$451~\mu H$
160 kHz	5200	1.736	569.97	11	514 μH
200 kHz	4000	8.339	76.00	5	73 μH
400 kHz	4000	2.000	79.15	5	73 μH

The acoustic projector is modeled as a capacitor device, and a resonance inductor is used to match the capacitance of the projector at the carrier frequency. Our prototype uses a coil inductor to achieve a specific inductance by controlling the number of wire turns. Taking the Btech 160 kHz transducer as an example, its capacitance is measured as C=1.736 nF. Given the carrier frequency  $f_c$ , the resonance inductance is calculated by [15]

$$f_c = \frac{1}{2\pi\sqrt{LC}}\tag{1}$$

Given the desired inductance L, the number of turns in a resonance coil inductor N satisfies [16]

$$L = A_L N^2 (2)$$

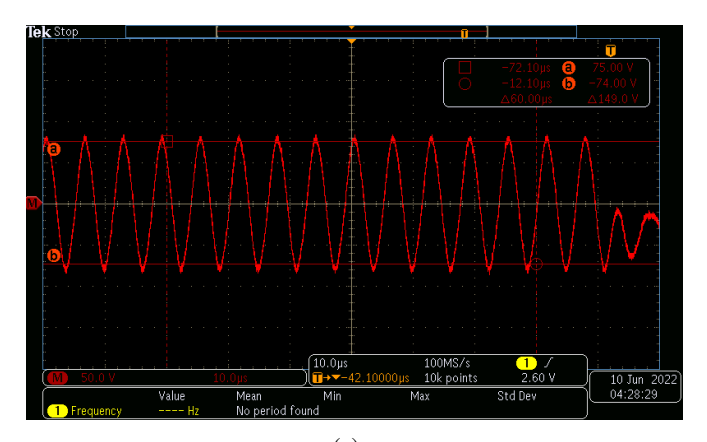
where  $A_L$  is the inductance factor in henry per turn-squared. Two sizes of the ferrite cores 3C91 are used in our prototype, which P22/13 core has an inductance factor  $A_L$  of 5200 nanohenry per turns-square [17] and P18/11 core has an inductance factor  $A_L$  of 4000 nanohenry per turns-square [18].

Using (1) and (2), the matching inductor for the targeted carrier frequencies and their corresponding numbers of turns are computed in Table I. The hand-made coil maybe less accurate than machine-made coils and the measured inductance is also shown in the table.

The LC resonance circuit serves as a low-pass filter and the high-order harmonics in the rectangular waves of the transformer output are filtered out, which further increases the voltage on the projector. Four different PA boards were made to verify the amplification ability for very-high frequency transmission. Extensive lab tests measured the outputs of the transducers. The results of 160 kHz and 400 kHz pure carriers are shown in Fig. 5, where Fig. 5a shows the voltage applied on the 160 kHz projector with a peak-peak voltage of 149 V, and Fig. 5b shows the output voltage applied on the 400 kHz projector with a peak-peak voltage of 168 V.

#### III. Low-Noise Amplifier (LNA)

The receiver front-end circuit consists of an LNA and a level shifter. The LNA amplifies the weak signal received from the hydrophone and filters the out-of-band noise and interference. The level shifter serves as a driver for the ADC and introduces a 1.5 V DC offset to meet the ADC's 0–3 V input range. As shown in Fig. 1, our prototyped LNA uses an instrumentation amplifier, a fixed-gain amplifier, a bandpass filter [19] and a level shifter. The instrumentation amplifier is characterized by low noise, low distortion, high input impedance, and high common-mode rejection ratio (CMRR) which meets the requirements of accuracy and stability as the



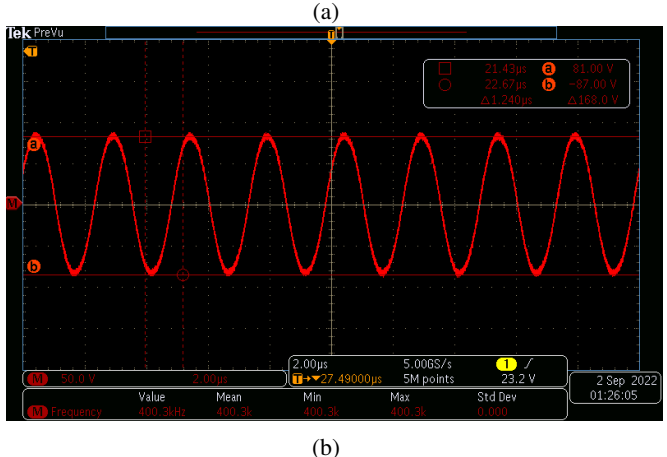


Fig. 5: Voltage applied on the transducers: (a) 160 kHz carrier and (b) 400 kHz carrier.

first stage amplifier. The selected instrumentation amplifier provides a gain of 26 dB and can take single-ended or differential inputs from the hydrophone. The fixed-gain amplifier at the second amplification stage uses the negative feedback inverting configuration of an operational amplifier to provide an additional 31 dB gain. Theoretically, the proposed LNA provides a total of 57 dB amplification gain. The bandpass filter ADA4807-4 from Linear Technologies is an eighth-order Butterworth filter.

For different carrier frequencies, the bandpass filter design uses a tool from Analog Devices [20] to identify the component values of the eighth-order Butterworth filter. If a desired frequency response is specified, the tool computes the values of external capacitors and resistors for ADA4807-4. Since the EIA (Electrical Industries Association) standard resistor/capacitor values have to be used for hardware implementation, the computed values of resistors and capacitors are replaced by their nearest E96 official values with 1 % tolerance. Note the E-series standard defines the resistor values in a decade based on

$$v_n = \text{round}\left(\sqrt[m]{10^n}\right) \tag{3}$$

where m is the E series number which determines the number of values in a decade and is related with the tolerance, and

 $n = 0, \dots, m - 1$ . For E96 series, m = 96.

Next, the obtained component values were brought into LTspice, a high-performance SPICE simulator software from Linear Technologies, to obtain the simulated frequency response. For example, the frequency response of the filter with a center frequency of 160 kHz and a bandwidth of 28 kHz is specified in the filter design tool of Analog Devices, as shown in Fig. 6a, while the simulated response by LTspice is shown in Fig. 6b. The simulated results agreed well with the designed responses.

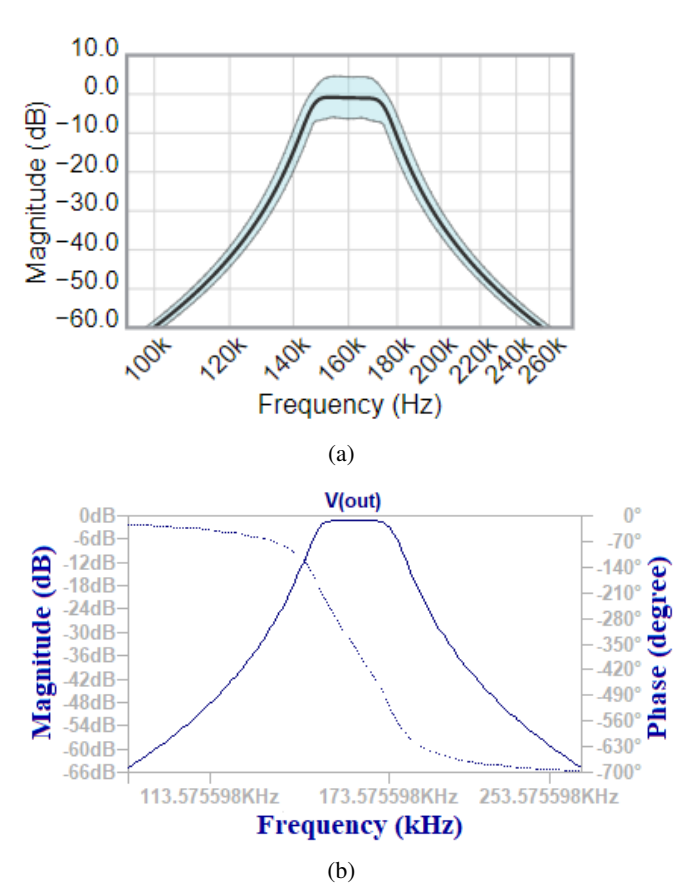


Fig. 6: The desired and simulated frequency responses by (a) filter design tool of Analog Devices; (b) LTspice simulator

Prototype boards were made for all four frequency bands and the lab tests used a function generator and an oscilloscope. The function generator provided a pure sine wave at low voltage with its frequency varying across the desired frequency band at a step of 2 kHz. The oscilloscope measured the outputs of the LNA board. As a test result, the minimum input voltage is 2 mV peak-peak. The frequency response is computed as shown in Fig. 7. Over a wide range of frequencies 145 kHz – 175 kHz, the LNA prototype achieved more than 52 dB amplification gain, but the passband was less flat than the simulated response. We found it difficult to achieve a flat response over a wide frequency band and chose to tolerate a slightly lower gain for the lower frequency end since the acoustic channels attenuate more on high frequency signals.

Similar results were obtained for the receiver front-end boards of all carrier frequencies.

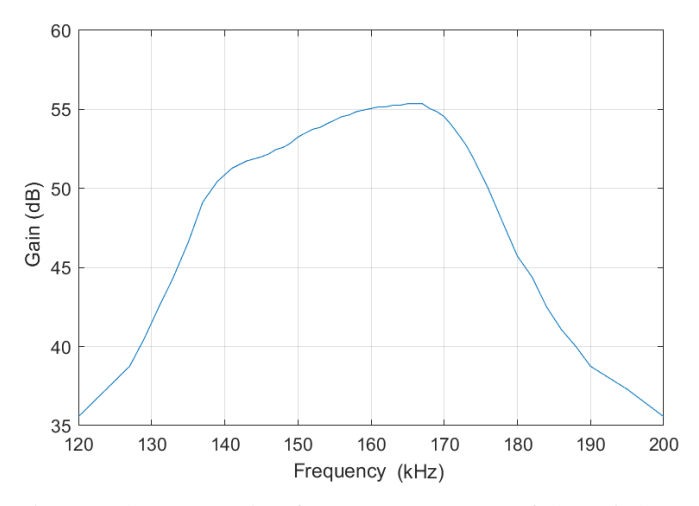


Fig. 7: Lab test results: frequency response of the 160 kHz LNA

#### IV. FIELD EXPERIMENTS

The transmitter and receiver front-end circuits have been tested extensively in the field too. The test setups are shown in Fig. 8a and Fig. 8b, respectively, where both the transmitter and receiver were powered by 3-cell LiPo batteries, respectively.

The transmitter generates Binary Phase-shift keying (BPSK) modulated data with a symbol rate of 20 kilo-symbol-persecond from the controller which was made by the Nvidia Jetson NX and a custom-made modulator [6] . The transmitter front-end board is powered with  $V_{cc}=12$  V, yielding 149 V peak-to-peak on the transducer. This is 75% of the maximum voltage of the transducer. The transmitted signal contains a pilot of 2047 bits pseudo-random-noise (PN) sequences, a gap with a duration of 255 symbols, then an 8191 bits PN sequence as payload.

The receiver front-end circuits output to an ADC board which connects to the Xilinx Field Programmable Gate Array (FPGA) development kit Zedboard. The ADC can achieve a sampling rate of 2 Msps and is programmable through the FPGA and the received data is transferred to a host laptop via the Ethernet cable.

The experiments were conducted at the Marina of the Nockamixon State Park, as shown in Fig. 9. The experiments were conducted in June – August 2022 normally during the early morning hours when the water temperature was relatively low and the boat traffic was minimum. The transmitter was placed inside a waterproofing container and the projector was dropped from a speedboat and placed 2 feet beneath the water surface. The receiver remained on the dock with the hydrophones dropped 2 - 4 feet below the water surface. The Tx-Rx distances were gradually increased at a step of a hundred meters. The boat was stopped when the transmitted



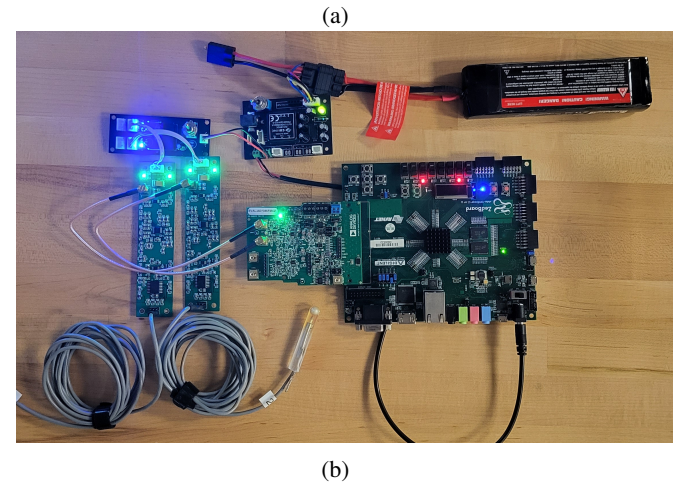


Fig. 8: Experiment setup for (a) transmitter and (b) receiver

signals were recorded at the receiver. A GPS on the boat was used to measure the distance from the dock.

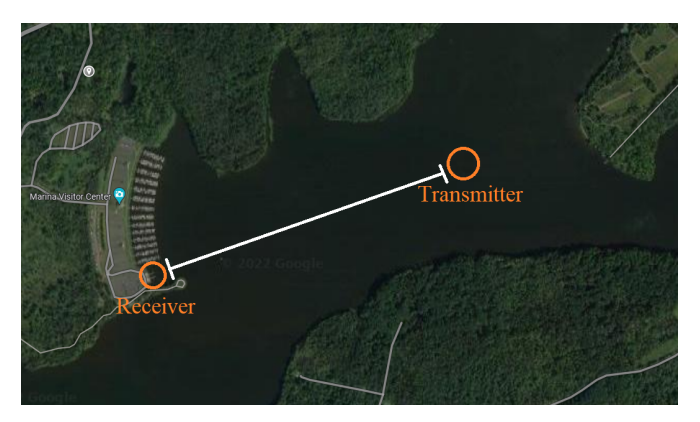


Fig. 9: Test site at the Nockamixon State Park, PA, USA

The results of the 160 kHz system is presented here. The data collected at distances of 500 m, 800 m and 1000 m are shown in Fig. 10. The pilot and the payload can be identified in figures on the left column, while the BPSK modulation is shown in the figures on the right column. The signal power was computed with the data corresponding to the pilot and payload,

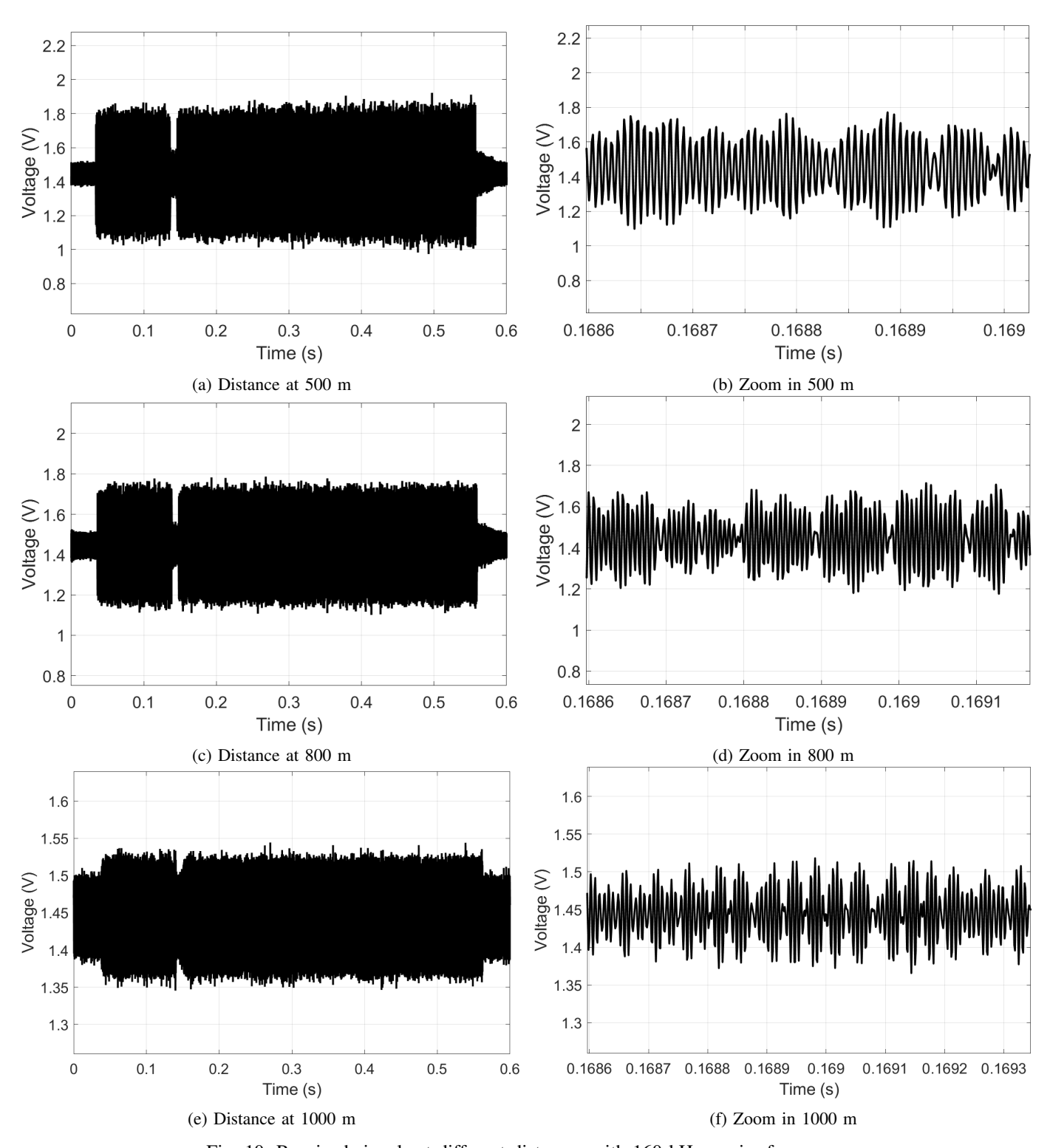


Fig. 10: Received signals at different distances with 160 kHz carrier frequency.

and the noise power was computed using the segments before the pilot block. At a distance of 500 meters, the received signal was much stronger than the noise achieving an SNR of 9 dB, as shown in Fig. 10a. As the distance reached 800 meters, the SNR decreased to 7dB, as shown in Fig. 10c. For the distance of 1000 meters, the SNR was 3.5 dB, as shown in Fig. 10e,. As the distance increased, the strength of the received signal decreased, but the noise level remained roughly the same. This lead to a decrease in the SNR which is predicted.

### V. CONCLUSION AND FUTURE WORK

The transmitter and receiver front-end circuits for ultrahigh-frequency UWA have been studied and tested for 115 kHz to 400 kHz. The field test results show that the 160 kHz system can achieve 3.5 dB received SNR at 1000 meters Tx-Rx distance in a lake environment. With a good coding and Turbo equalization scheme, the receiver would be able to decode the information bits at the low SNR region, making the ultrahigh-frequency bands a promising means to enable Internet of Underwater Things.

Future work will focus on reducing the noise figure, improving the receiver sensitivity, and adding automatic voltage control (AVC) circuits in the PA and the LNA, respectively.

#### ACKNOWLEDGMENT

The authors would like to thank Dr. Jun Yong for his tutorial on analog circuit design and Dr. Aijun Sun for sharing his 160 kHz transducers.

## REFERENCES

- M. Stojanovic, "Recent advances in high-speed underwater acoustic communications," *IEEE Journal of Oceanic Engineering*, vol. 21, no. 2, pp. 125–136, 1996.
- [2] T. J. Hajenko and C. R. Benson, "The high frequency underwater acoustic channel," in OCEANS'10 IEEE SYDNEY, 2010, pp. 1–3.
- [3] M. Stojanovic, "On the relationship between capacity and distance in an underwater acoustic communication channel," SIGMOBILE Mob. Comput. Commun. Rev., vol. 11, no. 4, p. 34–43, oct 2007. [Online]. Available: https://doi.org/10.1145/1347364.1347373
- [4] Y. R. Zheng, C. Edwards, F. Zhang, L. Emokpae, M. Pan, N. Mahmoudian, L. Emokpae, and M. Manteghi, "NSF workshop on Advancing Underwater Cyber Infrastructure for Blue Science," 2021. [Online]. Available: https://www.blue-uci2021.org
- [5] J. Li and Y. R. Zheng, "Hardware and software co-design of a single-carrier modulation (SCM) acoustic communication system," in OCEANS 2021: San Diego-Porto. IEEE, 2021, pp. 1–6.
- [6] X. Zhu and Y. R. Zheng, "Technologies for acoustic multiple-input multiple-output (mimo) transmission through a serial peripheral interface (spi) bus," 2022, patent Application Serial No 17745019.
- [7] J. Ingraham, Z. Deng, X. Li, T. Fu, G. McMichael, and B. Trumbo, "A fast and accurate decoder for underwater acoustic telemetry," *Review of Scientific Instruments*, vol. 85, pp. 074903–074903, 07 2014.
- [8] P.-P. J. Beaujean, E. A. Carlson, J. Spruance, and D. Kriel, "Hermes a high-speed acoustic modem for real-time transmission of uncompressed image and status transmission in port environment and very shallow water," in OCEANS 2008, 2008, pp. 1–9.
- [9] X. Xu, S. Zhou, K. Mahmood, L. Wei, and J.-H. Cui, "Study of class-d power amplifiers for underwater acoustic ofdm transmissions," in 2013 OCEANS - San Diego, 2013, pp. 1–3.
- [10] I. Kim, H. Kim, F. Griggio, R. L. Tutwiler, T. N. Jackson, S. Trolier-McKinstry, and K. Choi, "Cmos ultrasound transceiver chip for high-resolution ultrasonic imaging systems," *IEEE Transactions on Biomedical Circuits and Systems*, vol. 3, no. 5, pp. 293–303, 2009.

- [11] J. Honda and J. Adams, "Application notes an-1071: Class d audio amplifier basics," https://www.infineon.com/dgdl/an-1071.pdf? fileId=5546d462533600a40153559538eb0ff1, Feb 2005.
- [12] J. C. (Auth.), AC Power Conditioners. Design and Application. Elsevier Science, 1990.
- [13] Vishay, "Power mosfet basics: Understanding gate charge and using it to assess switching performance," https://www.vishay.com/doc?73217.
- [14] FDD86326 N-Channel Shielded Gate PowerTrench MOSFET, Onsemi, 2010. [Online]. Available: https://www.onsemi.com/pdf/datasheet/ fdd86326-d.pdf
- [15] H. Arai, M. Inaba, T. Ishigohka, H. Tanaka, K. Arai, M. Furuse, and M. Umeda, "Fundamental characteristics of superconducting fault current limiter using lc resonance circuit," *IEEE Transactions on Applied Superconductivity*, vol. 16, no. 2, pp. 642–645, 2006.
- [16] M. Bartoli, A. Reatti, and M. Kazimierczuk, "High-frequency models of ferrite core inductors," in *Proceedings of IECON'94 - 20th Annual Conference of IEEE Industrial Electronics*, vol. 3, 1994, pp. 1670–1675 vol.3.
- [17] Core P22/13-3C91, Ferroxcube, 2016. [Online]. Available: https://www.ferroxcube.com/upload/media/product/file/Pr\_ds/P22\_13.pdf
- [18] Core P18/11-3C91, Ferroxcube, 2019. [Online]. Available: https://www.ferroxcube.com/upload/media/product/file/Pr\_ds/P18\_11.pdf
- [19] C. Shi, "Improved design of high frequency bandpass filter based on LTC1562-2," in ", vol. 40, no. 88. Journal of Shanghai Ship and Shipping Research Institute, 2017.
- [20] A. F. Wizard. Analog devices ahead of what's possible. [Online]. Available: https://tools.analog.com/en/filterwizard/